

Vortex breakdown in a three-dimensional swirling flow

By E. SERRE AND P. BONTOUX

LMSNM, FRE 2405 CNRS/Universités d'Aix-Marseille, IMT La Jétée-Technopôle de
Château-Gombert, 38 rue Frédéric Joliot-Curie, 13451 Marseille cedex 20, France
serre1@l3m.univ-mrs.fr

(Received 30 April 2001 and in revised form 12 November 2001)

Time-dependent swirling flows inside an enclosed cylindrical rotor–stator cavity with aspect ratio $H/R = 4$, larger than the ones usually considered in the literature, are studied. Within a certain range of governing parameters, vortex breakdown phenomena can arise along the axis. Very recent papers exhibiting some particular three-dimensional effects have stimulated new interest in this topic. The study is carried out by a numerical resolution of the three-dimensional Navier–Stokes equations, based on high-order spectral approximations in order to ensure very high accuracy of the solutions.

The first transition to an oscillatory regime occurs through an axisymmetric bifurcation (a supercritical Hopf bifurcation) at $Re = 3500$. The oscillatory regime is caused by an axisymmetric mode of centrifugal instability of the vertical boundary layer and the vortex breakdown is axisymmetric, being composed of two stationary bubbles. For Reynolds numbers up to $Re = 3500$, different three-dimensional solutions are identified. At $Re = 4000$, the flow supports the $k = 5$ mode of centrifugal instability. By increasing the rotation speed to $Re = 4500$, the vortex breakdown evolves to an S-shaped type after a long computational time. The structure is asymmetric and gyrates around the axis inducing a new time-dependent regime. At $Re = 5500$, the structure of the vortex breakdown is more complex: the upper part of the structure takes a spiral form. The maximum rotation speed is reached at $Re = 10\,000$ and the flow behaviour is now chaotic. The upper structure of the breakdown can be related to the spiral-type. Asymmetric flow separation on the container wall in the form of spiral arms of different angles is also prominent.

1. Introduction

The motion of a viscous fluid contained in a closed cylinder, with a rotating disk lid, poses an attractive example of confined swirling flow. The many unresolved features of these kinds of flows in the laminar regime (see the review by Shtern & Hussain 1999) make their study both valuable and interesting. On other hand, this class of flow is also attractive as a vehicle for studying the transition to turbulence in finite-dimensional systems (Sorensen & Christensen 1995). This is particularly so for numerical studies, because the flow is completely closed and consequently the boundary conditions are well defined.

The major characteristics of the flow are known to be determined by two dimensionless parameters: the aspect ratio ($L = H/R$) and the rotational Reynolds number ($Re = \Omega R^2/\nu$), where H and R are, respectively, the height and the radius of the cylinder, Ω the angular velocity of the top endwall, and ν the kinematic viscosity of the fluid.

One of the particular interests of this type of flow is that the confined vortex can undergo breakdown for certain combinations of (L, Re) . In such cases, the vortex breakdown phenomenon occurs as an abrupt change in the structure of the vortex core (Benjamin 1962) and typically develops downstream into a recirculatory 'bubble' or a helical pattern. These phenomena, characterized by a stagnation zone in the flow, are of both fundamental and industrial interest. The physical interest lies mainly in the understanding of the origin and the appearance of these stagnation zones as well as in the examination of physical relations for flows with concentrated vorticity which are believed to play a crucial role in the onset of turbulence. Beyond the fundamental interest, there are also several potentially interesting practical applications associated with vortex breakdown. In particular, vortex breakdown occurs in swirling combustion chambers, in the channel-cavity configuration inside a turbine air cooling system (Owen & Pincombe 1979) or above delta and duck wings of fighter aircraft at high angles of attack (Peckam & Atkinson 1957). In the latter case, vortices separated from the wings can break down in the pressure field and causes instabilities. It is of interest to destroy these vortices to improve the handling of the aircraft or to stabilize the flames (Syred & Beer 1974).

No generally accepted theory exists that can explain the occurrence of vortex breakdown and the transition between different types of breakdown (see Shtern & Hussain 1999 for the different theoretical approaches). Some researchers include the development of a recirculatory zone and flow reversal in the vortex breakdown definition, making the vortex breakdown into an internal flow separation (Leibovich 1978). However, flow reversal does not necessarily occur in helical and turbulent vortex breakdown (Sarpkaya 1995). Nevertheless, this definition is currently considered in most cases in confined cavities, in which the vortex breakdown is often assimilated into one or more recirculation bubbles following the pioneering experimental investigations of Escudier (1984).

Escudier (1984) showed that several recirculation bubbles may exist on the main vortex axis and mapped out the steady and unsteady flow regions in the (Re, L) -plane, $L \leq 3.5$ (see figure 1, §4). He observed in the steady regime that the flow remains axisymmetric to a high degree of accuracy. Even after a considerable penetration into the unsteady domain of the stability diagram, the departure from axisymmetry is negligible, at least for aspect ratio $L \leq 3$. These first observations justified most numerical studies carried out with an axisymmetric model. Lugt & Haussling (1982) performed the first numerical study of swirling confined flow that reproduced the occurrence of breakdown. Subsequent investigations have accurately described the structure of the steady axisymmetric states (Lopez 1990; Lopez & Perry 1991). These studies were recently completed by the topological approaches of Brons, Voigt & Sorensen (1999, 2001) in a closed cylinder with co- and counter rotating end-covers and in the case of a cylinder with a rotating bottom and a free surface, respectively. Assuming the flow to be axisymmetric, these authors obtained a list of possible bifurcations of streamline structures from varying the parameters (Re, L) . These bifurcations are shown to be of a purely topological nature and are not related to changes in stability of the steady flow. For higher Reynolds numbers, Brons *et al.* (2001) have also numerically investigated the transition to a time-dependent solution and shown that the stability limit for steady flow is established as a Hopf bifurcation. This result using the finite difference code developed by Daube *et al.* (1985), had already been obtained in the numerical work of Daube & Sorensen (1989) in which they indicated that the transition in a cylinder of aspect ratio $L = 2$ occurs through a supercritical Hopf bifurcation for $Re \simeq 2400$. The linear stability analysis of Gelfgat,

Bar-Yoseph & Solan (1996) also demonstrated this result for a steady axisymmetric flow in a cavity of aspect ratio ($L = 2.5$); a Hopf bifurcation has been found near $Re = 2700$, and the most unstable mode has been found to be axisymmetric. Lopez & Perry (1991) and Sorensen & Christensen (1995) have reported and described the axisymmetric unsteady regimes: coalescing bubbles vortex breakdown are found in periodic and quasi-periodic regimes. The more recent combined experimental and numerical study of Stevens, Lopez & Cantwell (1999) extended the previous investigations into the unsteady flow regime far from the onset of the unsteadiness, and they demonstrated the existence of three oscillatory states with hysteretic jumps in a cavity of $L = 2.5$.

In spite of the numerous previous studies, controversies remain over the questions of the symmetry breaking of the flow and of vortex breakdown. Very recent experimental (Spohn, Mory & Hopfinger 1998) and numerical studies (Sotiroupolos & Ventikos 2001; Marques & Lopez 2001; Blackburn & Lopez 2000; Pereira & Sousa 1999) showed three-dimensional behaviour that arises in the structure of the vortex breakdown bubble and in the external vortex flow. Indeed, in the experiments of Spohn *et al.* (1998) and computations of Sotiroupolos & Ventikos (2001) the steady bubble is asymmetric and open. Moreover, recent computations of Marques & Lopez (2001) showed vortex breakdown in precession about the central axis for $Re = 2900$ ($L = 3$). Pereira & Sousa (2001) also obtained this precession motion for $Re = 3100$, portraying a fully non-symmetric behaviour but in a cavity with rotating cone. On the other hand, a recent three-dimensional numerical study of Blackburn & Lopez (2000) for $Re = 3500$ in a cylinder of aspect ratio $L = 2.5$, shows a symmetry breaking of the flow from a time-dependent axisymmetric state, leading immediately to modulated rotating waves with an azimuthal wavenumber $k = 5$.

The origin and the mechanism of the symmetry breaking have not yet been completely elucidated but could be related to the existence of asymmetric flow separation on the container wall (Spohn *et al.* 1998). Three-dimensional computations of Sotiroupolos & Ventikos (2001) seem to confirm these observations and show that these separation lines are due to the emergence of counter-rotating pairs of spiral vortices related to centrifugal instability of the boundary layer on the container wall. Nevertheless, these authors show that in their computations the separation of the sidewall layer is forced by the distorted structure of their Cartesian numerical grid. In contrast, Blackburn & Lopez (2000) and Marques & Lopez (2001), attribute this symmetry breaking to an instability of the swirling jet produced by the turning of the Ekman layer on the stationary vertical sidewall.

Escudier (1984) observed that the transition to a time-dependent flow for $L > 3.1$ was coupled with a precessing motion of the lower breakdown. In contrast, a recent linear stability analysis of Gelfgat, Bar-Yoseph & Solan (2001) shows that the basic state loses stability via a supercritical Hopf bifurcation to a $k = 4$ rotating wave and for a lower Reynolds number than Escudier. The numerical study of Marques & Lopez (2001) shows that the precession mode observed by Escudier (1984) is related to an instability (supercritical Naimark–Sacker bifurcation) of the $k = 4$ rotating wave state and not an instability of the steady axisymmetric basic state.

In the present investigation we bring some elements to this transition by solving the three-dimensional Navier–Stokes equations using a pseudo-spectral Chebyshev–Fourier method associated with a multi-step time scheme (Serre & Pulicani 2001). The spectral methods are particularly efficient in terms of accuracy with respect to the number of polynomials. The use of the Chebyshev collocation approximation is readily adapted to concentrating grid points close to the axis and in the thin

layers bordering the domain. Moreover, it is important to underline that this accurate method does not introduce fixed non-axisymmetric modes as in the case of curvilinear grids employed in finite-volume methods (for example Sotiroupolos & Ventikos 2001).

The transition to time-dependent regimes and three-dimensional behaviour are investigated in the same geometrical configuration as in the experiments of Escudier (1984). A cylinder with a larger aspect ratio than usually studied in the literature, $L = 4$, was selected, providing the expectation of a less stable flow, the axial confinement being reduced. The present study reveals some interesting new details of the closed swirling flow. The transition to an oscillatory flow is shown to occur through an axisymmetric bifurcation at $Re = 3500$. The time-dependent regimes are shown to be related to the vertical sidewall layer instability. Moreover, for a rotation speed up to $Re = 4500$, asymmetric vortex breakdown is found, associated with a precessing motion around the axis and with a shift from a bubble to a spiral type vortex breakdown.

The presentation is organized as follows. The mathematical model and numerical solution technique are described in §2 and §3. Numerical details and the verification of the numerical method on various well-documented test cases are presented in §4. The numerical results are given in §5 and are analysed in detail and compared with other investigations, both experimental and theoretical. Conclusions and discussion of further investigations are presented in §6.

2. Mathematical model

The equations governing the flow in this configuration are the three-dimensional Navier–Stokes equations written in velocity–pressure formulation, together with the continuity equation and appropriate boundary and initial conditions. It is convenient to write these using a cylindrical polar coordinate system (r, z, θ) , relative to a stationary observer with the origin at the centre of the cylinder. The velocity components are $V = (u, v, w)$ respectively, and p is the pressure. The scales for the dimensionless variables of space, time and velocity are $[H/2, \Omega^{-1}, \Omega R]$, respectively. The dimensionless axial and radial coordinates are $z = 2z^*/H$, $z \in [-1, 1]$ and $\bar{r} = 2r^*/H$, $\bar{r} \in [0, 2/L]$, respectively. The radius \bar{r} has been normalized on $[-1, 1]$, a requisite for the use of Chebyshev polynomials: the normalized variable is r with $r = (\bar{r}L - 1)$.

No-slip boundary conditions apply at each impermeable wall. Thus $u = w = 0$ on all rigid walls. For the azimuthal velocity, the boundary conditions are $v = 0$ on the stator ($z = \bar{z} = -1$) and $v = 0.5 \times (1 + r)$ on the rotating disk ($z = \bar{z} = 1$). The junction of the stationary cylinder with the rotor involves a singularity of the azimuthal velocity, as previously noted by Serre, Crespo del Arco & Bontoux (2001*a*). This singular condition expresses a physical situation where there is a thin gap between the edge of the rotating disk and the stationary sidewall. Unless this singularity is treated appropriately, spectral methods may have severe difficulties dealing with it. In order to regularize this condition, the boundary layer function, $v_\mu = \exp(-(z - 1))/\mu$ has been employed, where μ is an arbitrary shape parameter. It was shown for equivalent Reynolds numbers in Serre & Pulicani (2001) that this function with $\mu = 0.006$ provides a reasonable representation of experimental conditions, while retaining spectral accuracy.

The initial condition corresponds to no motion in the meridian plane and to a linear shear profile for the azimuthal velocity:

$$u = w = 0, \quad v = 0.25 \times (1 + r)(1 + z) \quad \text{for} \quad -1 \leq r, z \leq 1.$$

3. Numerical method

The numerical solution is based on a pseudo-spectral collocation-Chebyshev in both radial and axial directions (r, z) , and considering the 2π -periodicity of the solution in this configuration a Fourier–Galerkin method is used in the azimuthal direction (see Canuto *et al.* 1988). The choice takes into account the orthogonality properties of Chebyshev polynomials and, in particular, provides exponential convergence – referred to as spectral accuracy (Gottlieb & Orszag 1977). The high-order accuracy of these methods ensures an accurate description of the secondary flows of weak intensity compared to the external basic flow (as in the vortex breakdown recirculation zone). Moreover, the use of the Gauss–Lobatto collocation corresponding to the extrema of the Chebyshev polynomials of high degree, N and M in the radial and axial directions respectively, directly ensures high accuracy of the solution inside the very thin wall layers and in the neighbourhood of this axis.

The differential equations are exactly satisfied at the Gauss–Lobatto collocation points, $(r_i, z_j) \in [-1, 1] \times [-1, 1]$:

$$r_i = \cos(i\pi/N), \quad z_j = \cos(j\pi/M) \quad (i = 0, \dots, N \quad j = 0, \dots, M).$$

The approximation of flow variables $\Psi = (u, v, w, p)$ and their derivatives is derived from the following truncated series:

$$\Psi_{NMK}(r, z, \theta, t) = \sum_{p=K/2}^{K/2-1} \sum_{n=0}^N \sum_{m=0}^M \hat{\Psi}_{nmp}(t) T_n(r) T_m(z) e^{ip\theta} \quad \text{for } \left\{ \begin{array}{l} -1 \leq r, z \leq 1 \\ 0 \leq \theta \leq 2\pi \end{array} \right\},$$

$$\frac{\partial^q \Psi_{NMK}}{\partial r^q}(r_i, z_j, \theta_k, t) = \sum_{\eta=0}^N dr_{i\eta}^{(q)} \Psi_{NMK}(r_\eta, z_j, \theta_k, t),$$

$$\frac{\partial^q \Psi_{NMK}}{\partial z^q}(r_i, z_j, \theta_k, t) = \sum_{\xi=0}^M dz_{j\xi}^{(q)} \Psi_{NMK}(r_i, z_\xi, \theta_k, t),$$

where $dr_{ij}^{(q)}$ and $dz_{ij}^{(q)}$ correspond to the coefficients of the matrix of first and second derivatives ($q = 1, 2$) and where $\theta_k = 2\pi k/K$, $k = 0, \dots, K - 1$, are azimuthal points. An expansion of these coefficients based on the sinus function is used to reduce the round-off error. T_n and T_m are Chebyshev polynomials and $\hat{\Psi}_{nmp}$ are the spectral coefficients defined by

$$\hat{\Psi}_{nmp}(t) = \frac{1}{K} \frac{1}{c'_n} \frac{1}{c'_m} \sum_{k=0}^{K-1} \sum_{i=0}^N \sum_{j=0}^M \frac{1}{c_i c'_j} \Psi(r_i, z_j, \theta_k, t) T_n(r_i) T_m(z_j) e^{-ip\theta_k}$$

with $c_0 = c_N = c'_0 = c'_M = 2$ and $c_n = c'_m = 1$ for $n = 1, N - 1$ and $m = 1, M - 1$. The unknowns are required to be real $\Psi(r_n, z_m, \theta_k)$ in physical space. The physical conditions are explicitly taken into account at the boundaries.

The main computational difficulties come from the presence of the singularity at the axis ($\bar{r} = 0$) and the incompressibility constraint.

The first difficulty has been avoided with a variable transformation. The Fourier–Galerkin approximation leads to a set of elliptic equations for each Fourier wave to be solved in a two-dimensional domain depending on the two non-periodic directions. To obtain the solution of these equations boundary conditions are required on $\bar{r} = 0$ and $\bar{r} = 2/L$ (i.e. at the wall). At the wall, these conditions are given by the physical

	$u_{\max} \setminus u_{\min} $	$v_{\max} \setminus v_{\min} $	$w_{\max} \setminus w_{\min} $	σ
(a)				
$64 \times 96 \times 64$	0.156448 \setminus 0.0436474	1 \setminus 0.0273277	0.0576058 \setminus 0.137928	0.11512
$96 \times 96 \times 64$	0.156450 \setminus 0.0436470	1 \setminus 0.0273272	0.0576050 \setminus 0.137920	0.11510
$96 \times 122 \times 64$	0.156451 \setminus 0.0436471	1 \setminus 0.0273273	0.0576050 \setminus 0.137920	0.11511
(b)				
$64 \times 96 \times 64$	0.156448 \setminus 0.0436474	1 \setminus 0.0273277	0.0576058 \setminus 0.137928	0.1151215
$64 \times 96 \times 80$	0.156447 \setminus 0.0436474	1 \setminus 0.0273277	0.0576058 \setminus 0.137925	0.1151215
$64 \times 96 \times 128$	0.156448 \setminus 0.0436473	1 \setminus 0.0273276	0.0576057 \setminus 0.137925	0.1151212

TABLE 1. Mesh dependence of the solution characteristics in space and time at $Re = 4500$: (a) for different numbers of Chebyshev polynomials in the meridional plane (r, z) and (b) for different numbers of Fourier modes in the azimuthal direction. σ is the major angular frequency ($2\pi f$).

problem and at the axis they are imposed by the uniqueness of the solution, except for the first Fourier mode. Then, a change of dependent variables (Serre & Pulicani 2001) was used to enforce a boundary condition at the axis for this first Fourier mode:

$$\tilde{V} = \bar{r}V \quad \text{and} \quad \tilde{p} = \bar{r}p.$$

This variable change yields the conditions $\tilde{u} = \tilde{v} = \tilde{w} = \tilde{p} = 0$ at $\bar{r} = 0$. By applying the above variable changes, the Navier–Stokes equations transform to

$$\frac{\partial \tilde{V}}{\partial t} + A(\tilde{V}) = -G(\tilde{p}) + \frac{1}{Re}L(\tilde{V}),$$

$$D(\tilde{V}) = 0.$$

The operators after the change of variables are given in the Appendix.

It is easy to obtain V and p from \tilde{V} and \tilde{p} except at $\bar{r} = 0$, but the numerical method does not require this value. Nevertheless, in order to graphically represent the solution, different techniques for estimating the axis value are proposed in Serre & Pulicani (2001).

The second difficulty, due to the velocity–pressure coupling, has been overcome by the use of a projection scheme for time discretization. An improved version of the second-order pseudospectral method used in Raspo (1996) has been adopted. The improvement lies in the computation of the pressure predictor at each time step which allows a possible variation of the normal pressure gradient at the boundaries during the time integration. This version has been shown to reduce the slip velocity at the boundary and to produce second-order accuracy in time for the pressure.

The time scheme is semi-implicit second-order accurate. It corresponds to a combination of the second-order Euler backward differentiation formula and the Adams–Bashforth scheme for the nonlinear terms (Vanel, Peyret & Bontoux 1986).

4. Numerical details

The grid currently used is 64×96 in the (r, z)-plane with 64 Fourier modes in the azimuthal direction. This grid is fine enough for the rotation considered and corresponds to a compromise between the computational cost of the solution and the high accuracy required in the thin boundary layers and in the narrow region close to the axis. The time step incorporated is $\delta t = 10^{-2}$.

	Re	l/H	s/H	e/H
Escudier (1984)	1492	0.340	0.060	0.0410
Present results	1500	0.325	0.095	0.0547
Escudier (1984)	1854	0.210 (bubble 1)	0.160	0.113
		0.520 (bubble 2)	0.070	0.019
Present results	1850	0.208 (bubble 1)	0.179	0.120
		0.482 (bubble 2)	0.080	0.025

TABLE 2. Comparison of the characteristic lengths of the vortex breakdown with the experimental data available in a cavity of aspect ratio $L = 2$. Stationary solutions.

The solutions are grid independent. Different refinements have been tested and the time-dependent three-dimensional solution at $Re = 4500$ has been recomputed with higher resolutions. The space and time scales of the solution, as the maxima of the velocity components and the major frequency, respectively, differ by less than 0.1% with the refinement in the grid spacing. Some results are summarized in tables 1 and 2. Additional results regarding the accuracy of the numerical method are given by Serre & Pulicani (2001).

The three-dimensional nature of the solution is monitored through a time series of discrete spectral energies in each Fourier mode k ,

$$E_k = \frac{1}{N \times M} \sum_{i=1}^N \sum_{j=1}^M \hat{u}_k(r_i, z_j) \hat{u}_k^*(r_i, z_j),$$

where $\hat{u}_k(r_i, z_j)$ is the value of the k th Fourier mode of the velocity at the collocation points (r_i, z_j) , and \hat{u}_k^* is the complex conjugate of \hat{u}_k .

The performance of the solver has been optimized with respect to vector-parallel supercomputer, here a NEC SX5. The code was carried up to high-speed crest performances as we obtained about 6 gigaflops and a reference CPU time less as 10^{-6} second/mesh point/ δt . These code capabilities made possible the efficient computation of the high-resolution time-dependent solutions and allowed a sufficiently large simulation time to be reached to make the results of physical relevance.

4.1. Verification of the numerical method

To test the efficiency of our numerical method in accurately describing these problems, preliminary computations have been carried out for various well-documented test cases.

First, the method has been completely validated for selected parameters (L , Re) with respect to the previous experiments of Escudier (1984) (additional details about these cases are given by Serre & Bontoux 2001). The number and the position of the breakdown bubbles in stationary and oscillatory flows have been found to be in very good agreement with the experiments. We summarize the results that fit closely with the diagram map (figure 1): (i) the onset of the steady one-bubble vortex breakdown arises in the basic flow at $L = 2$ at about $Re = 1500$ in agreement with data; (ii) the two-bubble configuration is numerically determined between $Re = 1800$ and 2100 where a reverse transition is obtained; (iii) when further increasing Re from about 2600, the one-bubble configuration becomes unsteady up to $Re = 3000$ where a second reverse transition occurs towards an unsteady flow without breakdown; (iv) the two-bubble vortex breakdown is confirmed at intermediate $L = 2.5$ in the steady

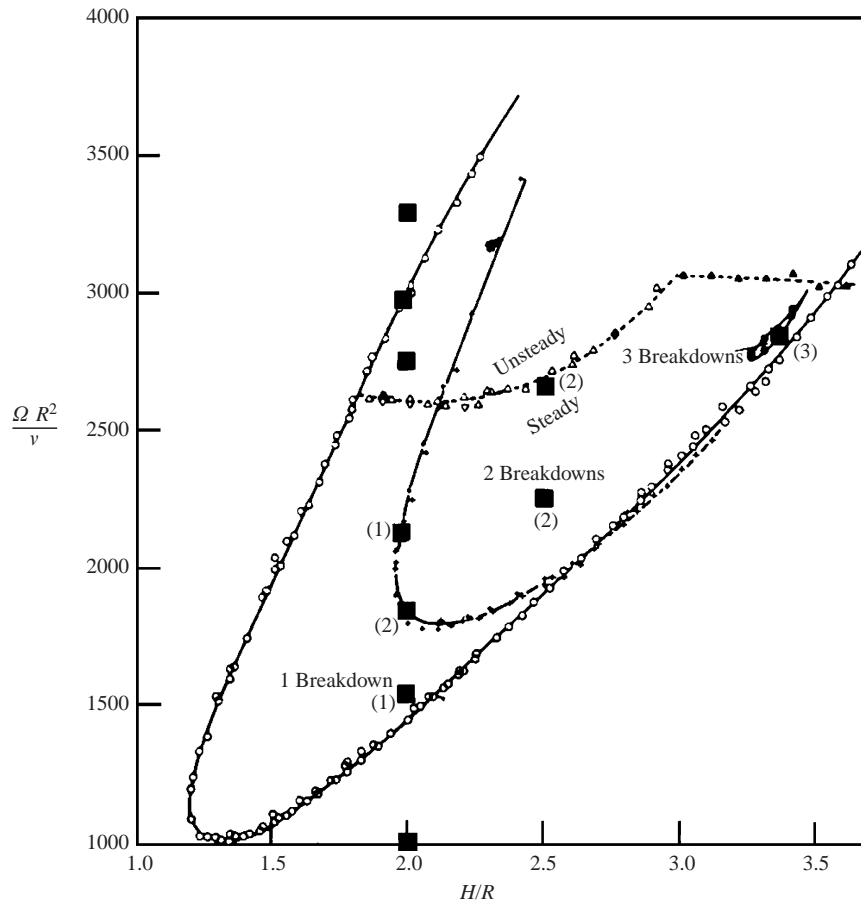


FIGURE 1. Comparison of flow states for some selected parameter combinations ($L = H/R$, Re) with the results obtained by Escudier (1984). Regimes where computations have been carried out are indicated by the black squares. The numbers in brackets give the number of bubbles numerically obtained.

regime; (v) the three-bubble configuration which corresponds to a very narrow area in the regime diagram from experiments, was also exactly determined at $L = 3.3$ at the same $Re = 2800$ as in the experiments. Moreover, the characteristic lengths (defined in figure 2) of the breakdown bubble in stationary flows inside a cavity $L = 2$ are found to be consistent with the available experimental data of Escudier (1984) (see table 2).

Secondly, we have considered the recent study of Marques & Lopez (2001) carried out for lower Reynolds numbers and a lower aspect ratio ($L = 3$) than the present one ($L = 4$). Both the bifurcations examined by Marques & Lopez (2001) have been reproduced but for slightly higher Reynolds numbers. The first transition to unsteady flow occurs via a Hopf bifurcation to a rotating wave $k = 4$ at $Re = 2900$ as in the computations of Marques & Lopez (2001) at $Re = 2730$. The vortex breakdown remains axisymmetric and the only departure from symmetry is in the meridian plane (figure 3). The secondary bifurcation takes place on increasing the rotation to $Re = 3100$, via a supercritical Naimark–Sacker bifurcation. A secondary frequency appears associated with the asymmetric mode, $k = 1$, absent at $Re = 2900$ and

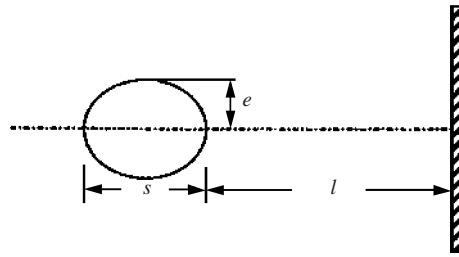


FIGURE 2. Sketch of the vortex breakdown bubble. Geometrical definition of the characteristic lengths of the vortex breakdown.

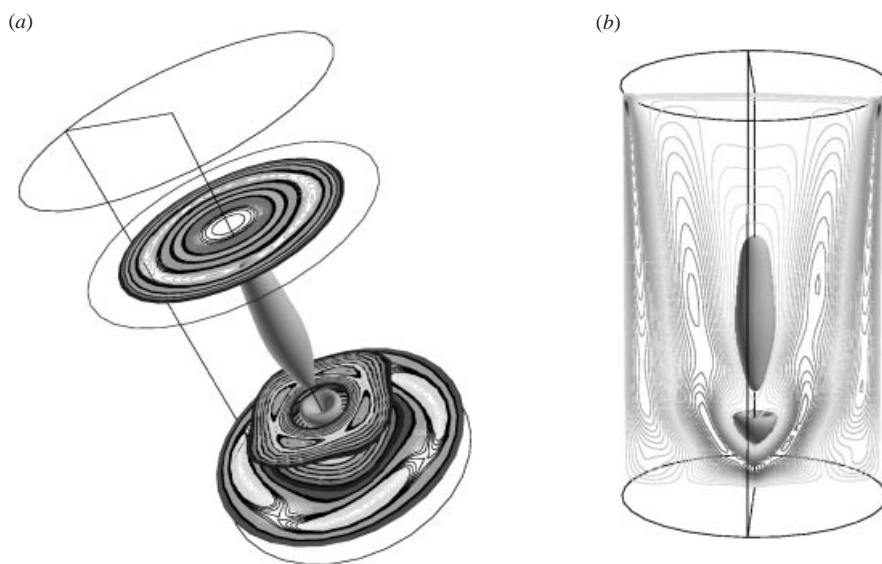


FIGURE 3. Flow solution at $Re = 2900$, $L = 3$. Iso-surface of axial velocity $w = 0$ showing an axisymmetric vortex breakdown with two bubbles, and iso-contours of axial velocity, w , in different selected (r, θ) - and (r, z) -planes, emphasizing the departure from symmetry only in the external flow of the vortex breakdown to a rotating wave $k = 4$. (a) $z^* = 3H/4$, $z^* = H/8$ and $z^* = H/10$, (r, θ) -planes; (b) $\theta = 0$, (r, z) -plane.

corresponding to the precession of the vortex breakdown. The spatial structure of this three-dimensional solution is similar to that computed by Marques & Lopez (2001) (figure 4). The Reynolds number $Re = 3100$, higher than the Reynolds number given by Marques & Lopez (2001), $Re = 2900$, is nevertheless closer to the one at which Escudier (1984) observed this precessing motion, $Re \gtrsim 3000$.

The complexity of the phenomena and of the dynamical processes that are simulated in this section, are considered to establish the quality and the accuracy of the solution solver and as a complete verification of the numerical method.

5. Results

The results presented in this section have all been obtained in a configuration of fixed aspect ratio $L = 4$.

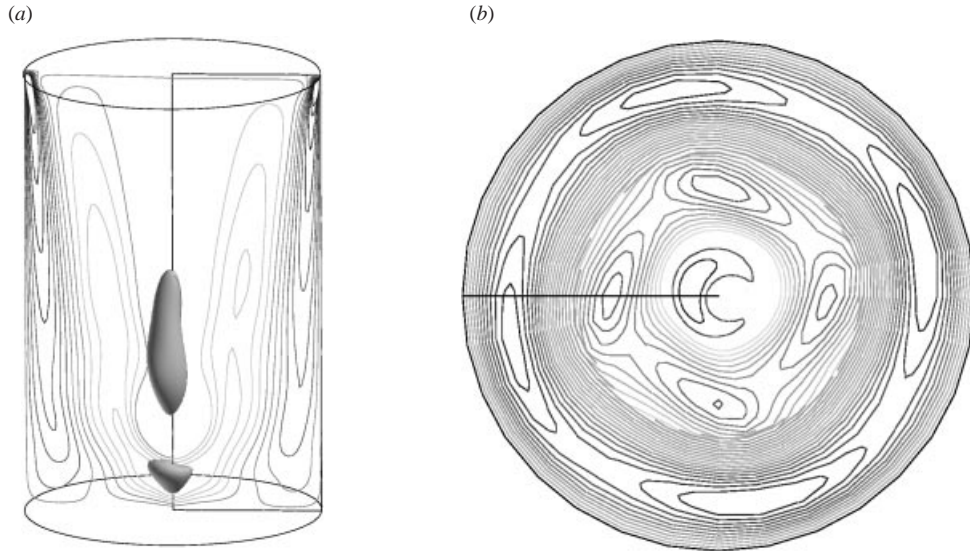


FIGURE 4. Flow solution at $Re = 3100$, $L = 3$. (a) Iso-surface of axial velocity $w = 0$ showing a three-dimensional vortex breakdown with two bubbles, and iso-contours of the axial velocity, w , in the meridional plane $\theta = 0$. (b) Iso-contours of w in the $z^* = H/5$ (r, θ) -plane emphasizing the departure from symmetry of both the external flow (to a rotating wave $k = 4$) and the vortex breakdown structure.

5.1. Basic state

Starting from an initial state at rest, the top endwall starts rotating instantaneously at $Re = 2500$. After a short transient time, all non-axisymmetric modes decayed until their energies E_k , $k \neq 0$, reached machine zero level. The resulting steady solution is axisymmetric without vortex breakdown and is considered to be the basic flow. The axisymmetry of this steady state is in good agreement with experiments of Escudier (1984) and the recent three-dimensional computations of Blackburn & Lopez (2000) and Marques & Lopez (2001).

Three-dimensional modes of the sidewall layer of a steady flow have been observed in experiments by Spohn *et al.* (1998) and in computations by Sotiropoulos & Ventikos (2001). Nevertheless, there are no contradictions with the present results, because these authors showed that these modes are forced either by the structure of their numerical grid or by the unavoidable non-axisymmetric disturbances arising, among others, from geometrical, thermal and dynamical experimental imperfections. Sotiropoulos & Ventikos (2001) only obtain the $k = 4$ spiral sidewall separation at $Re = 1850$, $L = 1.75$, when they use the Cartesian grid mapped onto the circle which has four singular points at the cylinder wall. Indeed, using a polar grid the steady state is axisymmetric for the same set of (Re, L) . This is consistent with the linear stability analysis for the three-dimensional perturbations of Gelfgat *et al.* (2001) which show, for the parameter range considered by Sotiropoulos & Ventikos (2001), that the steady flow is axisymmetric. In the present work, the use of collocation points in both (r, z) directions and equidistant points in the azimuthal direction is disturbance-free. Moreover, the numerical noise brought about by the spectral method is negligible.

Thus, the basic state at $Re = 2500$ is steady and axisymmetric but its structure is nevertheless non-trivial. As in the case of an infinite disk (see Greenspan 1969), when the upper disk is impulsively started, a thin Ekman boundary layer is formed which

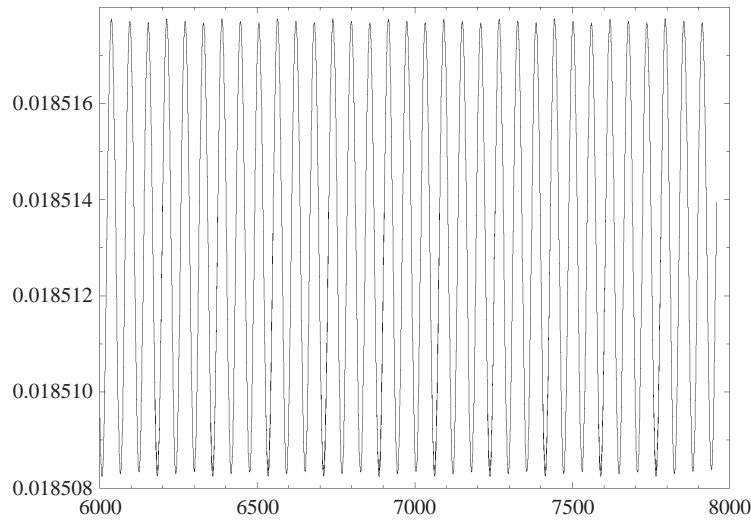


FIGURE 5. Time history of the axisymmetric mode ($k = 0$) of the spectral energy E_0 at $Re = 3500$. Periodic regime of frequency $\sigma = 0.105$.

acts as a pump (known as Ekman pumping) drawing in fluid axially and driving it away in centrifugal spirals. In a closed container, this fluid swirls along the stationary vertical wall to the stationary disk. Then, the fluid spirals inward in the Bödewadt layer and again turns in the axial direction towards the rotating disk. The flow inside the cylinder is thus driven and mainly determined by the axial component of the velocity and by the swirl component depending on the rotation speed of the disk, Ω .

Based on the above description, it is obvious that the transition of the global flow depends on the transition process inside each of the various three-dimensional boundary layers. The parameters governing the transition and the description of the instabilities in both Bödewadt and Ekman layers have also been previously investigated numerically in closed rotor–stator cavities ($L < 1$) by Serre *et al.* (2001*a*) and also in the case of an open rotating cavity with a radial throughflow by Serre *et al.* (2001*b*). There is no analytical description of the vertical sidewall layer because the stationarity of the cylinder leads to a too complex system of equations. Indeed, contrary to the rotating cylinder case (Stewartson layer) where the equilibrium between the viscous and the Coriolis forces completely determines the boundary layer, the Coriolis force suddenly vanishes at the wall in the present situation. Then, inertial nonlinear terms arise in the equilibrium of the viscous forces (see a review in Tomlan & Hudson 1971). Nevertheless, as is usual in the literature, we retain the term ‘Stewartson layer’ to denote the vertical layer in this work.

5.2. Onset of unsteadiness

Starting from $Re = 2500$, the solution at $Re = 3400$ remains steady without vortex breakdown. The first bifurcation to a time-periodic solution branch of frequency $\sigma = 0.105$ (where $\sigma = 2\pi f\Omega^{-1}$, the rotation frequency being unity) is obtained at $Re = 3500$. The amplitude of this solution is weak ($\approx 10^{-5}$) (figure 5) which suggests the closeness of the threshold. Nevertheless, due to prohibitive three-dimensional computational costs, the bifurcation point has not been resolved more precisely than within the Re range [3400, 3500].

The transition probably occurs through a supercritical Hopf bifurcation as shown

by the results of the linear stability analysis of Gelfgat *et al.* (1996) for cavities of aspect ratio, $1 \leq L \leq 3.5$ and, as suggested by the general behaviour of the flow response in the vicinity of the critical Reynolds number, the time-dependence is oscillatory with the amplitude decaying exponentially below the transition and there is no hysteresis cycle. This first bifurcation at $Re = 3500$ is axisymmetric over a large computational time of about 8500 (this is much larger than $\nu t^*/R^2 = 1.5$, generally accepted to reach an asymptotic state following the calculations of Tsiltverblit 1993 for an axisymmetric cylinder). The time evolution of the spectral energy E_k (for $k \neq 0$) shows that its amplitude remains close to the round-off error level of the computer. Moreover, this axisymmetric solution is stable with respect to a range of asymmetric disturbances of different wavelengths that were considered.

The flow undergoes breakdown with two axisymmetric recirculation bubbles of small size, separated by a rather large distance (figure 6a); the velocity vectors are also displayed at one given time instant. These recirculation bubbles are probably created when the steady flow becomes periodic because no bubble has been apparent in the steady regime at $Re = 3400$. Moreover, recirculation bubbles appearing after the onset of oscillatory instability were already reported in Gelfgat *et al.* (1996) for small aspect ratios. Nevertheless, more computations would be required close to the bifurcation to completely elucidate this point. Since the presence of a stagnation point in the central region of the flow has usually been defined as a positive identification of the breakdown zone, the surface $w = 0$ is considered when displaying the phenomenon. These bubbles are steady notwithstanding the oscillatory temporal evolution of the flow. Similar observations have been made in the experiments of Pereira & Sousa (1999) at $Re = 2700$ in a cylinder of aspect ratio $L = 3$ with a rotating cone. This shows that the time-dependent behaviour of the flow is not caused by the breakdown phenomenon and is not connected with it. In order to emphasize the oscillatory mode of instability responsible for the periodic behaviour, the time-dependent velocity fluctuations are computed at given instants with respect to the average flow solution. The vector field of the velocity fluctuation shows three pairs of counter-rotating rolls, of the same scale as the boundary layer thickness (figure 6b). The characteristics of these vortices and their location (they occur at the axial position $z = 3H/4$) suggest that their origin is related to the centrifugal instability, giving rise to the formation of vortex rings in the vertical sidewall boundary layer. Indeed, these structures emanate from a flow region where the centrifugal effects are the largest. These observations are in agreement with different previous theoretical, experimental and numerical studies (Tsiltverblit & Kit 1998; Escudier & Zenhder 1982; Pereira & Sousa 1999; Lopez, Marques & Sanchez 2001). Moreover, similar vortex rings related to the centrifugal instability were observed within a fraction of a second during an impulsive spin-down across the vertical layer of a rotor–stator cylinder ($L = 3.86$) by Weidman (1976). These rolls travel in the downstream direction, following the main inflow of the Bödewadt layer of the stationary disk and join together at the axis. Further, they are convected along the axis in the form of conical structures.

For $L = 4$ no data are available for comparison. Nevertheless, the characteristics of the solution are consistent with the available data for slightly smaller aspect ratios ($L \leq 3.5$). Although it is well known that the frequency of the solution varies considerably with the aspect ratio (see Stevens *et al.* 1999 for experiments and computations of these multiple states and their frequencies), we can see that the frequency of our solution is of the same order as that obtained in the recent computations of Blackburn & Lopez (2000) ($\sigma = 0.115$ for $L = 2.5$), and in the theoretical axisymmetric results of Gelfgat *et al.* (1996), $\sigma = 0.13$ for $L = 3.5$. The

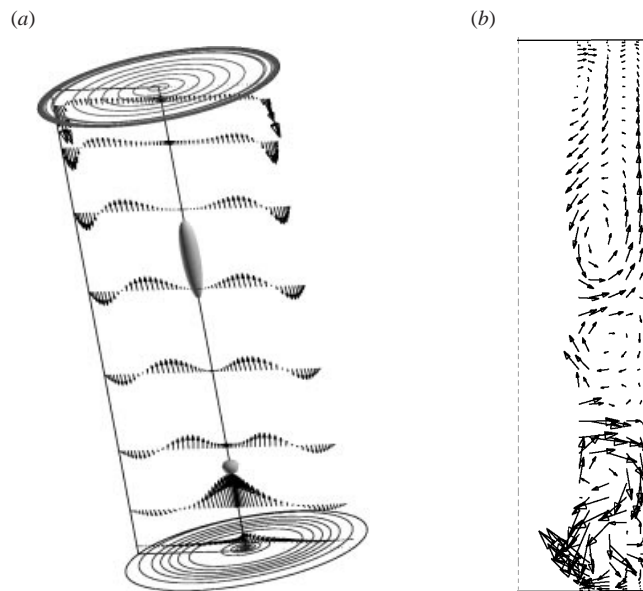


FIGURE 6. Axisymmetric time-periodic solution ($\sigma = 0.105$) at $Re = 3500$, $L = 4$. (a) Iso-surface of axial velocity, $w = 0$, showing two stationary bubbles. Velocity field in the meridional (r, z) -plane and iso-lines of the radial component of the velocity u emphasizing the axisymmetry of the flow close to the disks. (b) The velocity fluctuation field in the vertical sidewall layer showing four successive counter-rotating rolls superposed on the downstream flow and characteristic of the centrifugal instability.

Reynolds number of the transition, $Re = 3500$, is very close to the value obtained by extrapolating the data from the theoretical analysis of Gelfgat *et al.* (1996) (see figure 12a of their paper) but is larger than the value experimentally determined by Escudier (1984), $Re = 3000$, in cavities of aspect ratio in the range of $3 \leq L \leq 3.5$. This discrepancy can be only explained by asymmetric effects which are not observed here, because when the flows are axisymmetric, preliminary results in cavities of aspect ratio $L < 3$ are entirely consistent with the observations of Escudier (1984) (see figure 1 in §4.1).

This axisymmetric bifurcation is observed here for the first time in a cavity of large aspect ratio, $L = 4$, with reduced axial confinement effect. Indeed, Escudier's experimental observations ($3 \leq L \leq 3.5$) suggest that the basic state loses stability to a non-axisymmetric flow characterized by a precession motion of the breakdown; also, this precessing motion has been recently associated with an instability mode of wavenumber $k = 1$ by Marques & Lopez (2001). In contrast to the experimental work of Escudier, computations of these last authors show a supercritical Hopf bifurcation at $Re = 2730$ in a cavity of aspect ratio $L = 3$ but associated with a rotating wave with azimuthal wavenumber $k = 4$.

5.3. Subsequent bifurcations and three-dimensional flows

5.3.1. Three-dimensional flow associated with a rotating wave, $k = 5$

As the flow spins up at $Re = 4000$, starting from $Re = 3500$, a secondary bifurcation takes place to a rotating wave of azimuthal wavelength $k = 5$. The solution is time-dependent with two fundamental frequencies, $\sigma_1 = 0.108$, and a smaller one, $\sigma_2 = 0.08$. The three-dimensional mode of the centrifugal instability is clearly visible in the lower

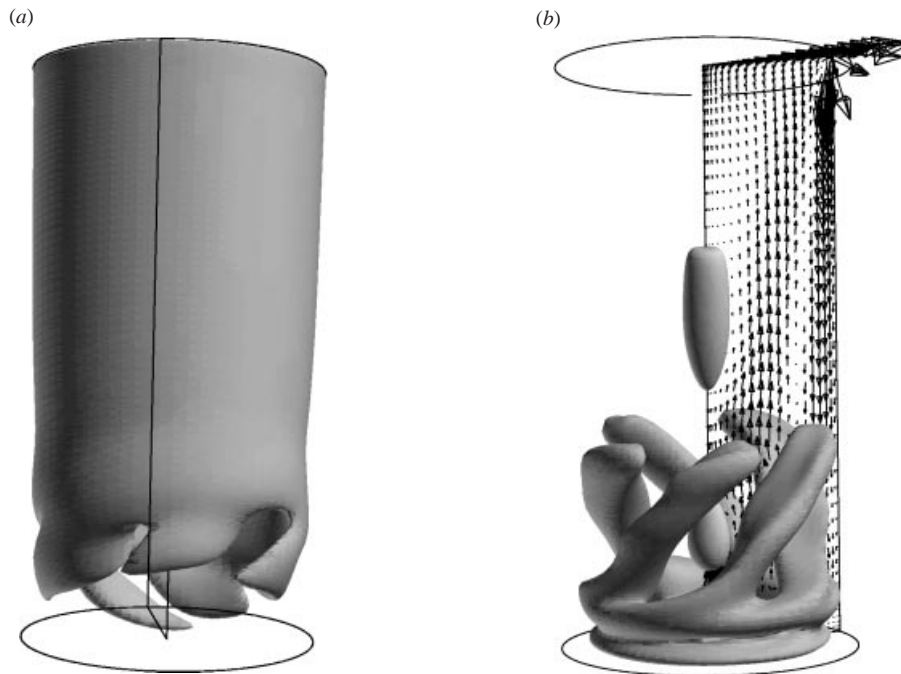


FIGURE 7. Azimuthal rotating wave of wavelength $k = 5$ at $Re = 4000$, $L = 4$. (a) Iso-surface of the radial velocity, u , showing the occurrence of spiral arms related to the centrifugal instability of the vertical boundary layer. (b) Iso-surfaces of the radial and axial components of the velocity in order to display the helical structures at the periphery and the axisymmetric vortex breakdown on the axis, respectively. The main flow direction in the meridional plane is indicated by the velocity field at one given time instant.

part of the vertical Stewartson layer. Figure 7(a) shows an isosurface of the radial component of the velocity which illustrates the spatial structure of the azimuthal wave in the Stewartson layer: rolls convected in spirals by the main flow occur at about $z = H/4$. These structures travel downstream to the stationary disk layer and reach the core region where they combine into a helical vortex pattern (figure 7b). The velocity vectors are also displayed at one specific time instant showing the main flow direction.

At this rotation speed, the vortex breakdown is composed of two recirculation bubbles as at $Re = 3500$ but of much larger size. These bubbles remain axisymmetric and are not affected by the structures related to the centrifugal instability. The plots at different short time instants show that the bubbles are steady. We can conclude that the unsteadiness of the solution is only related to the travelling motion of the centrifugal instability rolls. The largest frequency $\sigma_1 = 0.108$ remains close to that obtained at $Re = 3500$ ($\sigma = 0.105$) showing that the frequency of the temporally periodic axisymmetric state survives the bifurcation and that the $k = 0$ axisymmetric mode underlies the three-dimensional solution. Indeed, this frequency is related to the motion of the structures in the meridional plane, which means that the axial component of the phase velocity is very close to that of the $k = 0$ mode at $Re = 3500$. The occurrence of the frequency σ_2 corresponds to the precessing motion in the azimuthal direction of the $k = 5$ non-axisymmetric mode. The iso-lines of axial velocity displayed in figure 8 show the entire route of these structures. The presence of the vortices over the large height of the core region between the vortex breakdown

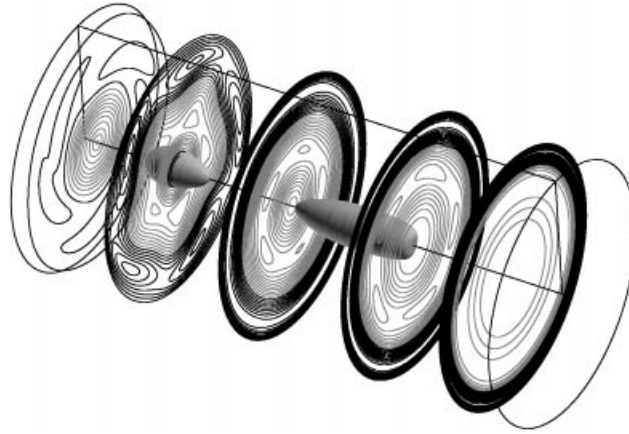


FIGURE 8. Axisymmetric vortex breakdown at $Re = 4000$, $L = 4$. Iso-lines of the axial component of the velocity in different selected (r, θ) -planes ($z = H/16, H/4, H/2, 3H/4, 3H/2$) showing the entire route of the vortices related to the $k = 5$ mode of the centrifugal instability and the feedback role played by the core region.

zone and the vertical boundary layer supports the idea of a positive feedback effect played by this flow region during the transition process. Tsitverblit & Kit (1998) have already demonstrated this effect of feedback when determining the critical Reynolds number of the transition, performing a linear stability analysis on different parts of the flow domain considered independently. This regime is noticeably similar to the one observed by Blackburn & Lopez (2000) in a cavity of smaller aspect ratio ($L = 2.5$) and for $Re = 3500$. There, a rotating wave ($k = 5$) occurs in the vertical boundary layer, from a time-periodic axisymmetric state and exhibits a spatial structure similar to the present one. Nevertheless, these authors did not show any evidence of vortex breakdown at these values of the parameters (L, Re).

5.3.2. Precessing S-shape vortex breakdown

Some asymmetries of the breakdown structure appear at $Re = 4500$ in the form of an 'S-shape' first noted by Escudier (1984) and which we use here to describe the first step of the vortex breakdown shift from the bubble to the spiral type. This is associated with a precessing motion of the two bubbles about the axis in the same direction as the main flow (figure 9a). This precession is observed after a long computational time ($\Omega t = 1800$) corresponding to the saturation of the three-dimensional non-zero modes and to the occurrence of a $k = 1$ mode.

The solution branch switches from the rotating wave $k = 5$ at $Re = 4000$ to rotating wave $k = 8$. The solution is time-dependent with a fundamental angular frequency, $\sigma = 0.115$, still close to the value observed at $Re = 3500$ as already noted above in §5.1. At this rotation speed, this solution is nevertheless unstable: the mode $k = 8$ grows first at about $\Omega t = 1500$ but a second $k = 1$ mode occurs at $\Omega t = 1800$. This mode grows very fast and reaches an amplitude four times greater than the $k = 8$ mode (figure 10). Both modes remain dominant (see for example in figure 10 the $k = 10$ mode of amplitude one order weaker than the $k = 8$ mode) over the computational time $\Omega t = 5300$, extracting energy from the axisymmetric mode (figure 10). The occurrence of these two dominant modes brings about significant modifications to the temporal behaviour of the solution and reveals the growth of new frequencies.

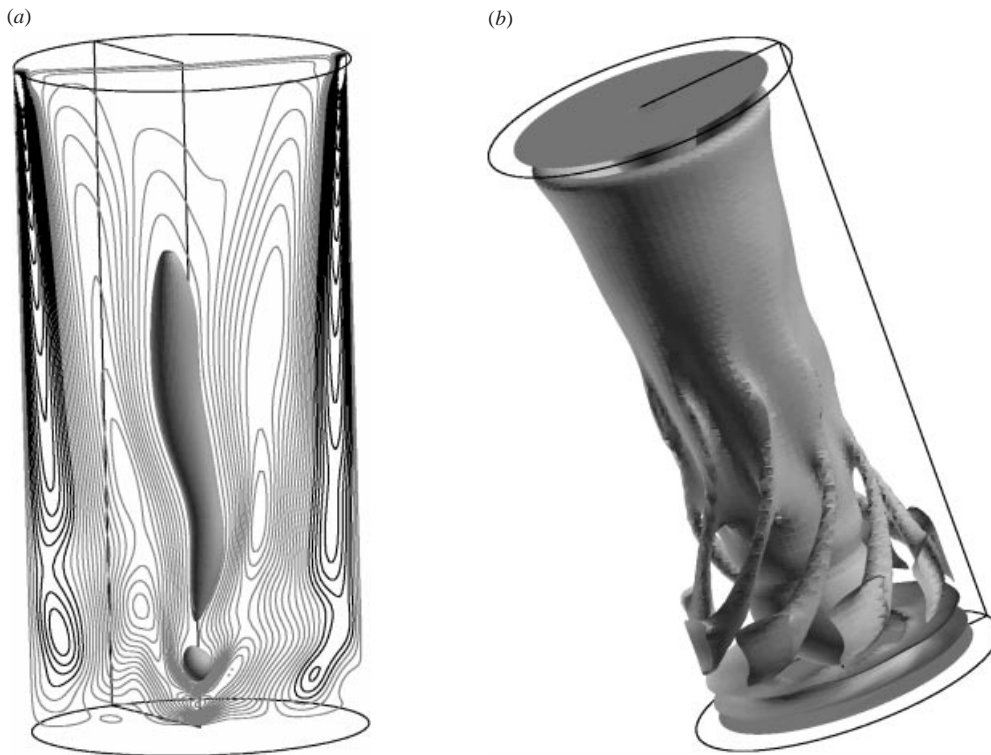


FIGURE 9. Three-dimensional solution at $Re = 4500$, $L = 4$. (a) Iso-surface $w = 0$ and iso-lines of the axial component of the velocity showing a precessing S-shape asymmetric vortex breakdown. (b) Azimuthal rotating wave associated with the $k = 8$ mode of the centrifugal instability. Iso-surface of the azimuthal component of the vorticity.

During the transient ($1500 \leq \Omega t < 1800$), the breakdown zone remains axisymmetric: the eight spiral arms in the Stewartson layer and the helical vortices located in the core region are the only departure from axisymmetry (figure 9b) showing that the $k = 8$ mode can be related to the instability of the sidewall layer. At $\Omega t = 1800$, corresponding to the saturation of the $k = 1$ mode, the upper structure of the breakdown rapidly mutates into an S-shape (figure 9a) and the two breakdowns simultaneously start to gyrate around the axis. The two breakdowns coexist during the whole oscillation process and the computations at different time steps show that their locations remain quite stationary in the axial direction. The asymmetry of the flow is now clearly visible in the meridian plane (figure 9a).

This result is consistent with the experimental observations of Escudier (1984) who noticed 'the precession of the lower breakdown structure' in oscillatory flows inside cavities of $L > 3.1$ (we recall that the 'lower structure' in the experiments of Escudier here corresponds to the upper structure because the rotor is in our geometry the top disk). This topology of the breakdown is also quite similar to that found by Pereira & Sousa (1999) at $Re = 3100$ inside a cavity in which the rotating top disk is a cone.

5.3.3. Precessing 'spiral-type' vortex breakdown

The rotation is instantaneously increased from $Re = 5500$. After $\Omega t = 1400$, the three modes $k = 1$, $k = 8$ and $k = 10$ now become dominant, exhibiting the strong nonlinear effect of the solution.

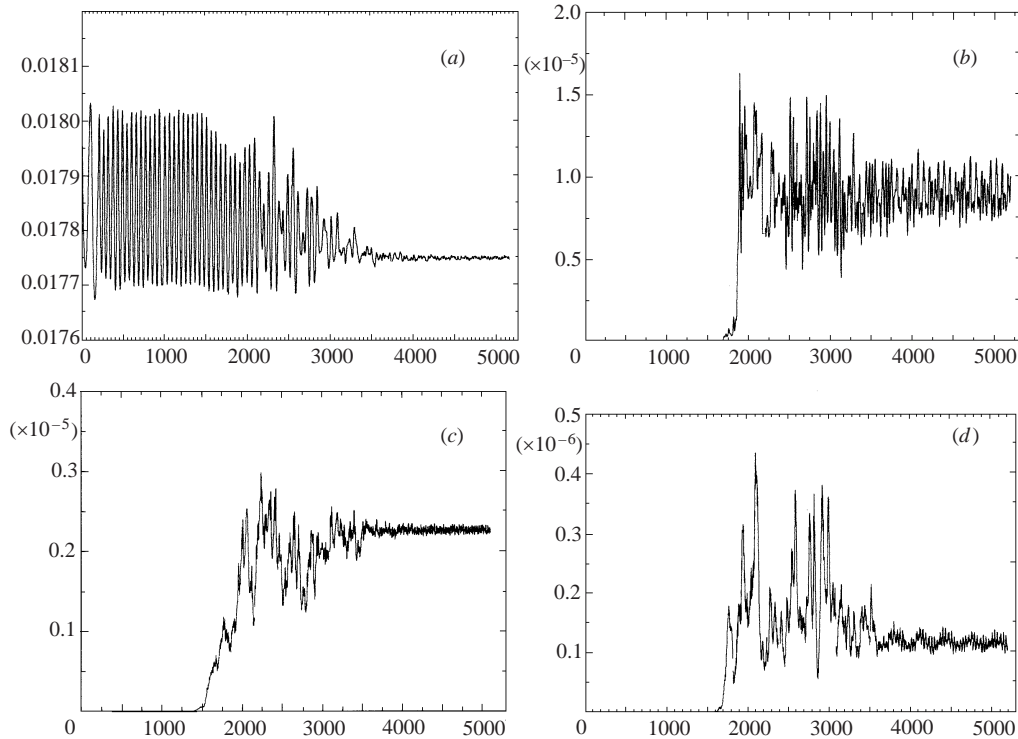


FIGURE 10. Time evolution of the spectral energy E_k (see §4) at $Re = 4500$. (a) axisymmetric mode of instability $k = 0$, (b) antisymmetric $k = 1$ mode, (c) three-dimensional $k = 8$ and $k = 10$ modes, respectively.

The dynamics of the vortex breakdown is illustrated at discrete time steps in figure 11 simultaneously with the fluctuations of the azimuthal component of the velocity in a meridian (r, z) -plane. The breakdown zone is composed of one structure only that gyrates around the central axis in counter-clockwise sense similarly to the main flow (figure 11). The rotation frequency of the breakdown is quite regular and equal to about twice the base frequency ($\sigma = 0.11$) related to the sidewall layer instability. Its topology is more complex than at $Re = 4500$ and confirms that an evolution occurs from the S-shape defined by Escudier (1984) to a vortex breakdown closer to the spiral-type. Leibovich (1978), visualizing the vortex axis with a dye filament, characterized this type as follows: ‘the spiral form is marked by a kink in the filament, followed by a corkscrew-shaped twisting of the dye’. It is clear from figure 11 that the spiral form occurs in the upper part of the breakdown. Moreover, the regularity of the precessing motion (nearly periodic) and the sense of the spiral, winding in the direction opposite to the base flow, are in good agreement with the observations of Brücker (1993).

The $k = 1$, $k = 8$ and $k = 10$ modes now have the same amplitude of about one thousandth that of $k = 0$. The spatial structures are shown for each of them, separately (figure 12). The entire flow region becomes three-dimensional except the upper half of the Stewartson layer dominated by the $k = 0$ mode. The $k = 8$ mode is concentrated in the lower half of the cavity, mainly inside the vertical boundary layer, showing that this mode is related to the centrifugal instability of the swirling jet above the cylinder wall. In contrast, both $k = 1$ and $k = 8$ modes are more concentrated

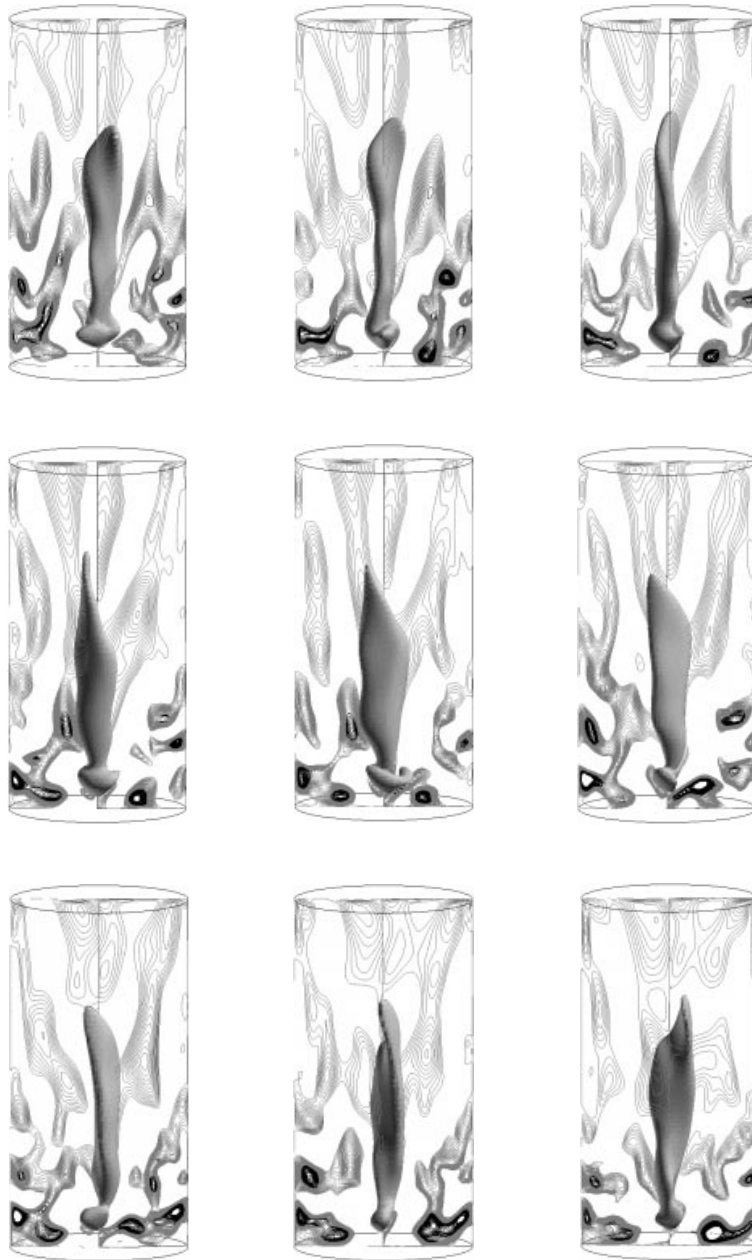


FIGURE 11. Precessing spiral-type vortex breakdown (iso-surface $w = 0$) at $Re = 5500$ at nine different time instants for $\Omega t \in [5500, 5608]$. The time step between each picture is $\Omega t = 12$. Iso-lines of the fluctuations of the azimuthal component of the velocity, v , showing the travelling counter-rotating rolls related to the three-dimensional mode of the vertical sidewall layer instability.

close to the stationary disc. The maximum of the $k = 1$ mode is located closer to the axis where the inflows of the Bödewadt layers on the right and on the left of the axis collide with each other. It is also of interest to note the extension of this mode both in the cavity region close to the axis, which corresponds to the breakdown zone, and also much higher in the cavity where the upward stream is pumped by the

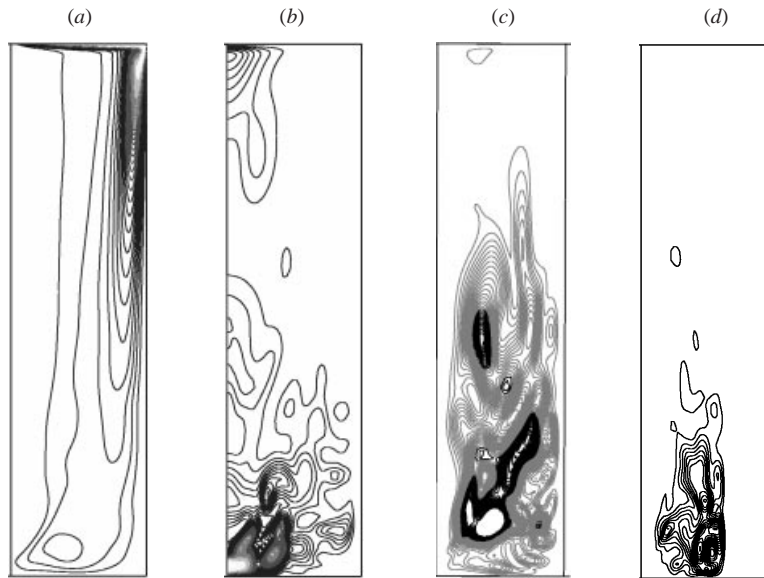


FIGURE 12. Iso-lines of the spectral energies in the (r, z) -planes showing the localization of the three-dimensional effects: (a) axisymmetric $k = 0$ mode, $[0; 10^{-2}]$; (b) $k = 1$, $[0; 9 \times 10^{-5}]$; (c) $k = 8$, $[0; 9 \times 10^{-5}]$; (d) $k = 10$, $[0; 9 \times 10^{-5}]$. The values in the brackets indicate the respective magnitude of the variation of the different energy modes, E_0 , E_1 , E_8 , E_{10} , respectively.

rotating top disc. This observation suggests that this $k = 1$ mode is responsible for the precessing motion of the breakdown. Its origin certainly requires further investigation but does not correspond to a Bödewadt instability. Indeed, at this rotation speed the flow region of the Bödewadt layer located at this distance from the axis is stable (see Serre *et al.* 2001a). The spatial extension of the $k = 0, 1, 8$ modes in the meridian plane is qualitatively similar to the case of Marques & Lopez (2001) in a cylinder of aspect ratio $L = 3$ at $Re = 2900$.

The maximum rotation speed considered in this paper was reached at $Re = 10\,000$. The temporal behaviour is now chaotic with several frequencies, indicating that more than three modes are dominant. The interaction among the various flow structures is then significantly much more complex. Nevertheless, it is clear from figure 13(a) that the breakdown is now close to the spiral-type defined by Leibovich (1978), particularly the upper part of the structure (corresponding to a 'stagnation surface $w = 0$ ') that is located completely outside the axis. The motion of these structures is also more complicated than at $Re = 5500$, because the precessing motion is doubled by an oscillatory motion (in translation) in the axial direction.

A zone of flow separation is observed in the upper part of the vertical sidewall layer, with the occurrence of a second series of eight spiral arms close to the rotating disc (figure 13b). This separation zone has already been observed in experiments by Spohn *et al.* (1998) in a cavity of aspect ratio $L = 2$. As in their experiments, the position of this zone remains remarkably stable at about $z = 2H/3$, throughout the computation. These spiral arms roll up in the same direction as those located closer to the stationary disc but they form a noticeably smaller angle (about 45°) with respect to the axial direction, emphasizing an important change in the wavelength. Weidman (1976) also observed changes in the wavelength of the centrifugal instability patterns during a quite slow spin-down. However, in contrast to the present computations and

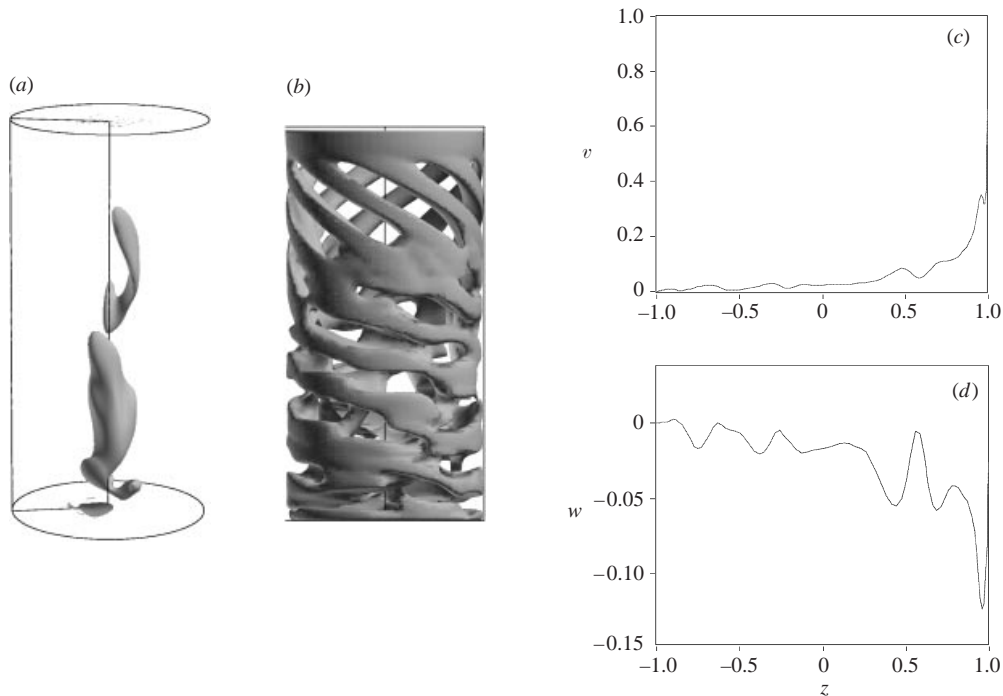


FIGURE 13. Three-dimensional flow at $Re = 10000$, $L = 4$. (a) Spiral-type vortex breakdown. Iso-surface of the axial velocity, $w = 0$. (b) Spiral structures of the instability of the vertical sidewall layer. Iso-surface of positive radial velocity ($u = 2 \times 10^{-3}$). (c, d) Axial profiles of the azimuthal velocity, v , and the axial velocity, w , near the vertical sidewall, respectively.

to the observations of Spohn *et al.* (1998), Weidman's experiments did not show a zone of flow separation because the angle of the spiral bands increased continuously all along the sidewall layer: the maximum helical angles of 70° to 75° were observed, much larger than the value obtained here.

This change in wavelength is due to a modification in the dynamics of the vortex flow that is apparent in the axial profiles of the main components of the velocity, v and w , inside the Stewartson layer (figures 13c and 13d). The upper part of the Stewartson layer corresponds to a flow region where both components of the velocity strongly decrease while the flow separates. In this flow region, the layer is similar to a strong-intensity thin jet developing along a concave stationary wall. Further, after the separation the velocity components are nearly independent of the axial coordinate z ; the intensity of the jet is weaker and the thickness increases bringing about the change in the wavelength.

It seems clear that these structures are also related to the centrifugal instability because at this Reynolds number the Ekman layer of the rotating disc is stable (Serre *et al.* 2001b). Nevertheless, we cannot definitively explain their occurrence at this location and at this high rotation speed. Indeed, at a lower rotation speed ($Re = 5500$), no structure has been observed in the main flow although the boundary layer profile (profile of w) already satisfies the so-called 'point-of-inflection criterion' (that a velocity profile which possesses a point of inflection is unstable) at this axial location. Then, as already noted above, a possible explanation can be given using the feedback role played by the central region. Indeed, contrary to the case at $Re = 5500$, the Ekman pumping is strong enough at $Re = 10000$: the three-dimensional structures

that travel upward in the central region are observed in the proximity of the rotating disc layer and are further transported to the upper part of the Stewartson layer. The central flow can then intensively transfer the disturbance from the location where the instability originates to the top of the cavity. As the profile is already unstable, the disturbance thus introduced brings about the growth of an instability mode characterized by spiral arms which are not observed at lower rotation speeds and are related to the centrifugal instability.

6. Conclusion

Fully nonlinear three-dimensional computations have been performed in a rotor–stator cylinder of large aspect ratio $L = 4$. The flow driven by the top rotating disc is studied for the first time for this value of L . The present study provides a new independent set of three-dimensional Navier–Stokes computations that are very helpful in the understanding of the transition from the steady axisymmetric flow to complex three-dimensional flow in this problem with well-defined boundaries. The transition to an axisymmetric periodic flow introduces a new bifurcation in the transition process for this flow in cavities of large aspect ratio $L > 3$. Moreover, the topology and the dynamics of asymmetric vortex breakdown have been detailed for the first time in this configuration.

The spectral numerical method associated with a thin grid mesh and coupled with a very efficient direct solver of the Navier–Stokes equations ensures high-order accuracy of the solutions. A relevant measure of this accuracy is the value of the velocity field divergence in order to check the incompressibility constraint (Serre & Pulicani 2001). In all the cases, this value is less than 10^{-11} within the domain and 10^{-5} at the boundaries. Thus, these very accurate numerical results would constitute a benchmark reference for other results obtained in the same configuration.

Our results show that the transition to a periodic regime at $Re = 3500$ occurs through an axisymmetric Hopf bifurcation. This axisymmetric bifurcation is observed here for the first time in a cavity of large aspect ratio. The transition process is brought about by an axisymmetric mode of instability originating from the vertical sidewall layer. This instability mode is related to the centrifugal instability and travelling counter-rotating vortices are observed in the Stewartson layer. The form of the perturbations and their location are reminiscent of Taylor–Görtler vortices with a superimposed vertical motion (travelling Taylor–Görtler vortices). The vortex breakdown is composed of two steady bubbles of small size, suggesting that they are not connected to the time-dependent behaviour of the flow.

For Reynolds number up to 3500, successive stable time-dependent flows are observed and different three-dimensional modes of instability are apparent. These modes are associated with the centrifugal instability (except the $k = 1$ mode which is associated with a jet-like instability) and characterized by spiral arms evolving in helical structures in the central region of the flow. For $Re = 4000$, a rotating wave of azimuthal wavelength $k = 5$ occurs. This branch is created as a secondary Hopf bifurcation from the first axisymmetric temporally periodic solution at $Re = 3500$. As shown in Blackburn & Lopez (2000) and in Marques & Lopez (2001) in cylinders of aspect ratios $L = 2.5$ and $L = 3$, respectively, this secondary bifurcation is a Naimark–Sacker bifurcation, i.e. a Hopf bifurcation from a time-periodic state. The vortex breakdown remains axisymmetric up to $Re = 4500$, for which a precessing motion about the axis of the vortex breakdown structure is obtained. This motion, originally observed by Escudier, is not related to an instability of the steady basic

state but corresponds to the growth of the $k = 1$ mode from the unstable $k = 8$ wave state. The spatial localization of the maximum intensity of this particular $k = 1$ mode when the jet rebounds from its collision at the axis on the stationary disc suggests that it originates from a jet instability. Nevertheless, in confined flows the location of the maximal disturbance may not coincide with the location of the origin of the instability. This point requires further investigation.

At $Re = 10000$, corresponding to the highest rotation speed considered in this work, the temporal behaviour of the flow is chaotic with several frequencies. A separation zone in the Stewartson layer of the vertical stationary cylinder is also observed, characterized by the occurrence of a second series of spiral arms with a different wavelength, located in a flow region closer to the rotating disc layer. A possible explanation of the origin of these structures is given, related to a feedback role played by the central region of the cylinder. At this rotation speed, the Ekman pumping is strong enough to transfer the structures of the instability from the bottom to the top of the cavity. These numerical simulations have also revealed the dynamics of the vortex breakdown in a cylindrical container. As the rotation speed increases, the vortex breakdown switches from a bubble to a spiral type at $Re = 10000$, i.e. from an axisymmetric to a three-dimensional structure. For all the Reynolds numbers considered, the spiral type (also called ‘S-shape’ in the first stage of the transition) has a precessing motion about the axis.

The computations were carried out on Nec SX5 supercomputer of IDRIS/CNRS (Orsay). The authors are grateful to Professors R. Peyret (CNRS/University of Nice), P. Le Quéré (CNRS/LIMSI Paris) and O. Daube (University of Evry, Paris) for fruitful discussions. We also wish to thank B. Launder (UMIST, Manchester) for his kind help in the writing of this work. The research was partly supported by the Réseau MFN (CNRS-DFG). A support for E. S. during the last stages of the submission by a C.N.E.S. postdoctorate grant is also acknowledged.

Appendix

Derivative operators after the variable change given in § 3 are as follows:

$$D(\tilde{V}) = \frac{1}{r} \frac{\partial \tilde{u}}{\partial r} + \frac{1}{r^2} \frac{\partial \tilde{v}}{\partial \theta} + \frac{1}{r} \frac{\partial \tilde{w}}{\partial z},$$

$$A(\tilde{V}) = [A(\tilde{V})_r, A(\tilde{V})_\theta, A(\tilde{V})_z]^T, \quad L(\tilde{V}) = [L(\tilde{V})_r, L(\tilde{V})_\theta, L(\tilde{V})_z]^T$$

with

$$A(\tilde{V})_r = \frac{\tilde{u}}{r} \frac{\partial \tilde{u}}{\partial r} + \frac{\tilde{v}}{r^2} \frac{\partial \tilde{u}}{\partial \theta} + \frac{\tilde{w}}{r} \frac{\partial \tilde{u}}{\partial z} - \frac{\tilde{u}^2 + \tilde{v}^2}{r^2}, \quad A(\tilde{V})_\theta = \frac{\tilde{u}}{r} \frac{\partial \tilde{v}}{\partial r} + \frac{\tilde{v}}{r^2} \frac{\partial \tilde{v}}{\partial \theta} + \frac{\tilde{w}}{r} \frac{\partial \tilde{v}}{\partial z},$$

$$A(\tilde{V})_z = \frac{\tilde{u}}{r} \frac{\partial \tilde{w}}{\partial r} + \frac{\tilde{v}}{r^2} \frac{\partial \tilde{w}}{\partial \theta} + \frac{\tilde{w}}{r} \frac{\partial \tilde{w}}{\partial z} - \frac{\tilde{u}\tilde{w}}{r^2},$$

$$L(\tilde{V})_r = \frac{\partial^2 \tilde{u}}{\partial r^2} - \frac{1}{r} \frac{\partial \tilde{u}}{\partial r} + \frac{1}{r^2} \frac{\partial^2 \tilde{u}}{\partial \theta^2} + \frac{\partial^2 \tilde{u}}{\partial z^2} - \frac{2}{Rer^2} \frac{\partial \tilde{v}}{\partial \theta},$$

$$L(\tilde{V})_\theta = \frac{\partial^2 \tilde{v}}{\partial r^2} - \frac{1}{r} \frac{\partial \tilde{v}}{\partial r} + \frac{1}{r^2} \frac{\partial^2 \tilde{v}}{\partial \theta^2} + \frac{\partial^2 \tilde{v}}{\partial z^2} + \frac{2}{Rer^2} \frac{\partial \tilde{u}}{\partial \theta},$$

$$L(\tilde{V})_z = \frac{\partial^2 \tilde{w}}{\partial r^2} - \frac{1}{r} \frac{\partial \tilde{w}}{\partial r} + \frac{\tilde{w}}{r^2} + \frac{1}{r^2} \frac{\partial^2 \tilde{w}}{\partial \theta^2} + \frac{\partial^2 \tilde{w}}{\partial z^2}.$$

For the pressure:

$$L(\tilde{p}) = \frac{\partial^2 \tilde{p}}{\partial r^2} - \frac{1}{r} \frac{\partial \tilde{p}}{\partial r} + \frac{\tilde{p}}{r^2} + \frac{1}{r^2} \frac{\partial^2 \tilde{p}}{\partial \theta^2} + \frac{\partial^2 \tilde{p}}{\partial z^2}, \quad G(\tilde{p}) = \left[\frac{\partial \tilde{p}}{\partial r} - \frac{\tilde{p}}{r}, \frac{1}{r} \frac{\partial \tilde{p}}{\partial \theta}, \frac{\partial \tilde{p}}{\partial z} \right]^T.$$

REFERENCES

- BENJAMIN, T. B. 1962 Theory of the vortex breakdown phenomenon. *J. Fluid Mech.* **14**, 593–629.
- BLACKBURN, H. M. & LOPEZ, J. M. 2000 Symmetry breaking of the flow in a cylinder by a rotating end wall. *Phys. Fluids* **12**, 2698–2701.
- BRONS, M., VOIGT, L. K. & SORENSEN, J. N. 1999 Streamline topology of steady axisymmetric vortex breakdown in a cylinder with co- and counter rotating end-covers. *J. Fluid Mech.* **401**, 275–292.
- BRONS, M., VOIGT, L. K. & SORENSEN, J. N. 2001 Topology of vortex breakdown bubbles in a cylinder with a rotating bottom and a free surface. *J. Fluid Mech.* **428**, 133–148.
- BRÜCKER, C. 1993 Study of vortex breakdown by particle tracking velocimetry. *Exps. Fluids* **14**, 133–139.
- CANUTO, C., HUSSAINI, M. Y., QUARTERONI, A. & ZANG, T. A. 1988 *Spectral Methods in Fluids Dynamics*. Springer.
- DAUBE, O., LOC, T. P., MONET, P. & COUTANCEAU, M. 1985 Ecoulement instationnaire décollé d'un fluide incompressible autour d'un profil : une comparaison théorie-expérience. *AGARD CP* 366.
- DAUBE, O. & SORENSEN, J. N. 1989 Simulation numérique de l'écoulement périodique axisymétrique dans une cavité cylindrique. *C. R. Acad. Sci.* **308** (II b), 463–469.
- ESCUDIER, M. P. 1984 Observations of the flow produced in a cylindrical container by a rotating end wall. *Exps. Fluids* 179–186.
- ESCUDIER, M. P. & ZENHDER, N. 1982 Vortex flow regimes. *J. Fluid Mech.* **115**, 105–121.
- GELFGAT, A. Y., BAR-YOSEPH, P. Z. & SOLAN, A. 1996 Stability of confined swirling flow with and without vortex breakdown. *J. Fluid Mech.* **311**, 1–36.
- GELFGAT, A. Y., BAR-YOSEPH, P. Z. & SOLAN, A. 2001 Three-dimensional instability of axisymmetric flow in a rotating lid-cylinder enclosure. *J. Fluid Mech.* **438**, 363–377.
- GOTTLIEB, D. & ORSZAG, S. A. 1977 *Numerical Analysis of Spectral Methods: Theory and Application*. SIAM.
- GREENSPAN, H. P. 1969 *The Theory of Rotating Fluids*. Cambridge University Press.
- LEIBOVICH, S. 1978 The structure of vortex breakdown. *Annu. Rev. Fluid Mech.* **10**, 221–246.
- LOPEZ, J. M. 1990 Axisymmetric vortex breakdown. Part 1. Confined swirling flow. *J. Fluid Mech.* **221**, 533–552.
- LOPEZ, J. M., MARQUES, F. & SANCHEZ, J. 2001 Oscillatory modes in an enclosed swirling flow. *J. Fluid Mech.* **439**, 109–129.
- LOPEZ, J. M. & PERRY, A. D. 1991 Axisymmetric vortex breakdown. Part 3. Onset of periodic flow and chaotic advection. *J. Fluid Mech.* **234**, 449–471.
- LUGT, H. J. & HAUSSLING, H. J. 1982 Axisymmetric vortex breakdown in rotating fluid within a container. *Trans. ASME: J. Appl. Mech.* **49**, 921.
- MARQUES, F. & LOPEZ, J. M. 2001 Precessing vortex breakdown in an enclosed cylinder flow. *Phys. Fluids* **13**, 1679–1682.
- OWEN, J. M. & PINCOMBE, J. R. 1979 Vortex breakdown in a rotating cylindrical cavity. *J. Fluid Mech.* **90**, 109–127.
- PECKAM, D. H. & ATKINSON, S. A. 1957 Preliminary results of low speed wind tunnel tests on a Gothic wing of aspect ratio 1.0. *Aeronaut. Res. Counc. Tech. Rep.* 1957, CP-508, TN No. Aero. 2504.
- PEREIRA, J. C. F. & SOUSA, J. M. M. 1999 Confined vortex breakdown generated by a rotating cone. *J. Fluid Mech.* **385**, 287–323.
- RASPO, I. 1996 Méthodes spectrales et de décomposition de domaine pour les écoulements complexes confinés en rotation. Doctorate Thesis, Université de la Méditerranée, Marseille (France).
- SARPAKAYA, T. 1995 Turbulent vortex breakdown. *Phys. Fluids* **7**, 2301–2304.
- SERRE, E. & BONToux, P. 2001 Eclatement tourbillonnaire dans une cavité rotor-stator cylindrique. *C. R. l'Acad. Sci. Paris* IIB **329**, 671–677.

- SERRE, E., CRESPO DEL ARCO, E. & BONTOUX, P. 2001a Annular and spiral patterns in flow between rotating and stationary disks. *J. Fluid. Mech.* **434**, 65–100.
- SERRE, E., HUGUES, S., CRESPO DEL ARCO, E., RANDRIAMAMPANINA, A. & BONTOUX, P. 2001b Spiral and circular instability patterns in an Ekman boundary layer flow. *Int. J. Heat Fluid Flows* **22**, 82–93.
- SERRE, E. & PULICANI, J. P. 2001 A 3D pseudospectral method for convection in a rotating cylinder. *Comput. Fluids* **30**, 491–519.
- SHTERN, V. & HUSSAIN, F. 1999 Collapse, symmetry breaking, and hysteresis in swirling flows. *Annu. Rev. Fluid Mech.* **31**, 537–566.
- SORENSEN, J. N. & CHRISTENSEN, E. A. 1995 Direct numerical simulation of rotating fluid flow in a closed cylinder. *Phys. Fluids* **7**, 764–778.
- SOTIROPOULOS, F. & VENTIKOS, Y. 2001 The three-dimensional structure of confined swirling flows with vortex breakdown. *J. Fluid Mech.* **426**, 155–175.
- SPOHN, A., MORY, M. & HOPFINGER, E. J. 1998 Experiments on vortex breakdown in a confined flow generated by a rotating disc. *J. Fluid Mech.* **370**, 73–99.
- STEVENS, J. L., LOPEZ, J. M. & CANTWELL, B. J. 1999 Oscillatory flow states in an enclosed cylinder with a rotating endwall. *J. Fluid Mech.* **389**, 101–118.
- SYRED, N. & BEER, J. M. 1974 Combustion in swirling flows. *Combust. Flame* **23**, 143–155.
- TOMLAN, P. F. & HUDSON, J. L. 1971 Flow near an enclosed rotating disk: analysis. *Chem. Engng Sci.* **26**, 1591–1600.
- TSITVERBLIT, N. & KIT, E. 1998 On the onset of unsteadiness in confined vortex flows. *Fluid Dyn. Res.* **23**, 125–152.
- VANEL, J. M., PEYRET, R. & BONTOUX, P. 1986 A pseudospectral solution of vorticity-streamfunction equations using the influence matrix technique. *Numerical Methods for Fluid Dynamics II* (ed. K. W. Morton & M. J. Baines), pp. 463–475. Clarendon.
- WEIDMAN, P. D. 1976 On the spin up and spin-down of a rotating fluid. Part 2. Measurements and stability. *J. Fluid Mech.* **77**, 709–735.